Measurement of the temperature-dependent optical constants of water ice in the 15–200 μm range

Daniel B. Curtis, Bhavani Rajaram, Owen B. Toon, and Margaret A. Tolbert

The real and imaginary refractive indices of water ice in the far infrared (IR) are used in the satellite interpretation of cloud properties as well as to obtain information on ice throughout the solar system. However, few measurements of these values exist. We have measured the real and imaginary refractive indices of water ice in the far IR every 10 deg over the temperature range of 106–176 K. Ice films ranging from 0 to 140 μm thick were grown by the condensation of water vapor onto a cold silicon substrate, and the film transmission was measured from 650 to 50 cm^{-1}. The thickness of the ice films was determined using optical interference from a reflected He–Ne laser (λ = 623.8 nm). The optical constants were then determined by simultaneously fitting the calculated spectra of films of varying thickness to their respective measured transmission spectra with an iterative Kramers–Kronig technique. The results are compared with previously measured data and show large discrepancies at some wavelengths while good agreement exists at others. Possible reasons for the differences are discussed. Our data clearly distinguish crystalline and amorphous ice. In addition, we note a slight shoulder in our spectra, which can be used to distinguish between cubic and hexagonal ice, although this distinction is difficult.

OCIS codes: 010.2940, 010.7340, 310.6860, 350.1270.

1. Introduction

Cirrus clouds, composed of water ice, play an important role in the Earth's climate system and have been identified as one of the most uncertain components in regulating the Earth's climate variability.[1,2] At temperatures that are typically found at the altitudes of cirrus clouds, the peak of the Planck function is in the far infrared (IR). Therefore accurate far-IR optical constants are crucial for the proper retrieval of the optical properties of cirrus clouds. In Fig. 1 we show the dimensionless extinction efficiency Q_{ext} that we calculated using Mie theory for a 50 μm ice particle and the IR optical constants in Warren's compilation.[3] For particles in the 50–100 μm size range typical of cirrus clouds, Q_{ext} of a single particle is largest in the far-IR region. At a given wavelength in the far IR, Q_{ext} and Q_{abs} are very sensitive to the size of cirrus cloud particles, making this frequency range a desirable one for probing optical properties of cirrus clouds.

Accurate optical constants are also crucial for IR astronomical applications. Water ice has been identified as a dominant building material for solid celestial bodies and as a component of dust in interstellar clouds. For example, water ice has been observed in the polar caps on Mars, in the outer solar system, and in interstellar dust.[4–12] The far-IR wavelengths are invaluable for the study of cooler objects, which emit at far-IR wavelengths. Furthermore, far-IR wavelengths are able to penetrate dust clouds within which star birth and death are observed to occur. Remote sensing of icy surfaces and atmospheres, especially using far-IR wavelengths, is currently experiencing rapid development. Figure 2 shows the frequencies at which observations have been made [Infrared Space Observatory (ISO) mission[13]] and will be made [Space InfraRed Telescope Facility (SIRTF), currently called the Spitzer Space Telescope, launched 25 August 2003, and Stratospheric Observatory for Infrared Astronomy (SOFIA) missions[14,15]]. Also plotted are the imaginary indices of

When this research was performed, D. B. Curtis, B. Rajaram, and M. A. Tolbert were with the Cooperative Institute for Research in Environmental Science and Department of Chemistry and Biochemistry, University of Colorado, Boulder, Colorado 80309. D. B. Curtis (daniel-curtis@uiowa.edu) is now with the Department of Physics and Astronomy and Department of Chemistry, University of Iowa, 217 IATL, Iowa City, Iowa 52242. O. B. Toon is with the Laboratory for Atmospheric and Space Physics and Program in Atmospheric and Oceanic Science, University of Colorado, Boulder, Colorado 80309.

Received 4 June 2004; revised manuscript received 30 December 2004; accepted 11 January 2005.

0003-6935/05/194102-17$15.00/0

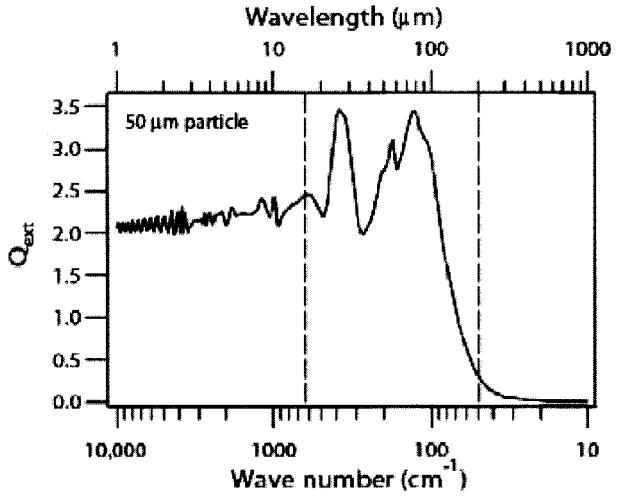

Fig. 1. Dimensionless extinction efficiency Q_{ext} calculated using Mie theory for a 50 μm particle and the IR optical constants in Warren's compilation.[3] The two vertical dashed lines mark the wavelength region that is covered by our experiments.

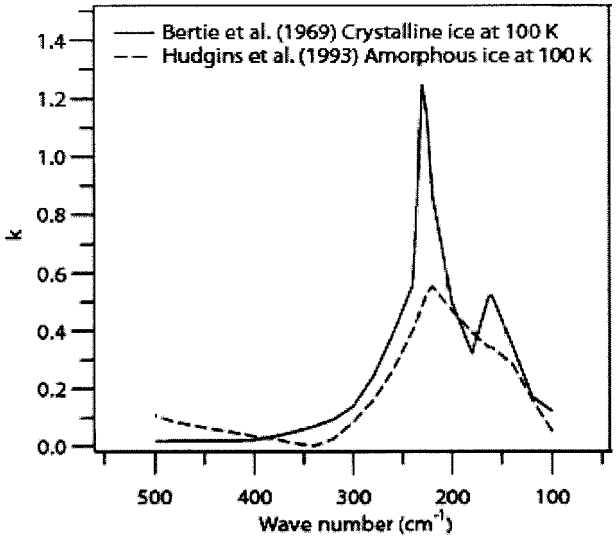

Fig. 3. Imaginary indices of refraction of crystalline ice I_c at 100 K from Bertie *et al.* (1969).[16] Imaginary indices of refraction of amorphous ice at 100 K from Hudgins *et al.* (1993).[21]

refraction of water ice from Warren's compilation[3] taken from Bertie *et al.*[16] It can be seen that the observational studies will cover wavelengths into the far IR. Therefore it is important to have accurate optical constants for water ice in the far IR to retrieve data from the observations. The vertical dashed lines delineate the wavelength range of the present study, which overlaps the observational wavelength ranges.

2. Far-Infrared Spectrum of Water Ice

During the past ten years several research groups have studied the temperature dependence of the far-IR spectra of water ice films that were formed by different methods.[17–20] The results of these studies

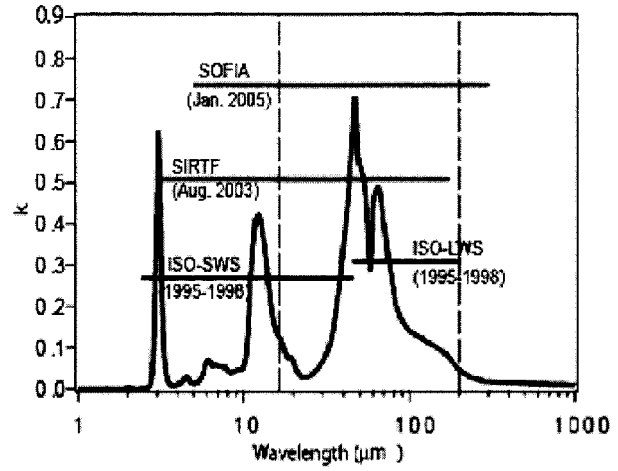

Fig. 2. Frequencies where observations were and will be made by various missions: ISO SWS (shortwave spectrometer), ISO LWS (long-wave spectrometer), SIRTF and Spitzer Space Telescope launched 25 August 2003, and SOFIA. These observation regions are overlaid on top of the imaginary indices of refraction of water ice from Warren's compilation. The vertical dashed lines mark the wavelengths that are covered by our experiments.

can be summarized as follows. Water ice when deposited on a substrate at temperatures at or below ~110 K is amorphous. The temperature at which the amorphous to crystalline phase change occurs has been observed to vary from 110 to 130 K depending on experimental conditions, in particular, the substrate on which the ice films were formed and the surface roughness of the substrate.[18] A sample spectrum of amorphous ice is shown in Fig. 3. It can be seen that amorphous ice has a single featureless broad absorption peak centered at ~215 cm^{-1}. When this ice is warmed above ~110 K, it undergoes an irreversible change to the cubic form, ice I_c, and when warmed above ~140 K it transforms irreversibly to the hexagonal form, ice I_h. A sample spectrum of crystalline ice in the far IR is shown in Fig. 3. The change from amorphous to cubic ice is accompanied by a frequency shift of the tranverse optical (TO) band maximum from ~215 to ~225 cm^{-1}. In addition, there is also a dramatic increase in the peak absorbance of this band, and the ~160 cm^{-1} longitudinal acoustic band becomes more prominent in the crystalline phase. The mid-IR of the cubic and the hexagonal forms of ice have previously been shown to be indistinguishable.[16] However, Bertie and Jacobs[22] showed that there is a slight difference in the far-IR spectra of cubic and hexagonal ice near 160 cm^{-1}.

It has further been shown that the crystalline phase spectra exhibit certain differences depending on whether the film was formed by warming up a film that was initially deposited at a lower temperature or by direct deposition of vapor at that temperature.[17] The most striking differences between the two cases are (1) the 225 and 160 cm^{-1} bands are narrower in the direct deposition case, and (2) the ratio of the 225–160 cm^{-1} peak absorbance is larger for the direct deposition case. Neither of these differences has been

Table 1. Summary of Far-IR Optical Constant Measurements Available in the Literature

Authors	Experiment	Sample Preparation	Phase of Ice	Substrate and Film Thickness
Bertie *et al.* (1969)[a]	Transmission, 100 K	Ice films formed by condensing water vapor on a cold window at 173 K, followed by cooling to 100 K	Always crystalline (I_h)	Polyethylene films from 0.8 to 27 mm
Hudgins *et al.* (1993)[b]	Transmission, 10, 100, 140 K	Deposited film at 10 K1, warmed to 100 and 140 K	Always amorphous	Polyethylene, 1.1 μm
Johnson and Atreya (1996)[c]	Transmission, 77, 100, 150 K	Film grown at 77 K, warmed to 150 K, then cooled to 100 K	Amorphous at 77 K, crystalline (I_c) at 100 and 150 K	Silicon, 10 μm
Trotta (1996)[d]	Transmission, 33–145 K	Film grown at 33 K, warmed during various thermal cycles	Crystalline (I_c)	Polyethylene, 14.3 μm (calculated from transmission)

[a]Ref. 16.
[b]Ref. 21.
[c]Ref. 4.
[d]Ref. 23.

quantified, and they appear to be dependent on experimental conditions.[19]

3. Summary of Available Measurements

Table 1 summarizes the currently available measurements of the optical constants of water ice in the far IR. These include data of Bertie *et al.*,[16] Hudgins *et al.*,[21] Johnson and Atreya,[4] and those of Trotta[23] (Warren[3] used Bertie *et al.* in his 1984 compilation). The data of Trotta[23] appeared in a dissertation and was also later published in Coustenis *et al.*,[12] but we refer to the dissertation data throughout this manuscript. The imaginary indices of refraction of crystalline ice films of Johnson and Atreya[4] and Bertie *et al.*[16] at 100 K and the crystalline ice films of Johnson and Atreya[4] and Trotta[23] at ~150 K are compared in Fig. 4(a). The imaginary index of refraction for amorphous ice of Hudgins *et al.*[21] at 100 and 140 K is shown in Fig. 4(b). Also shown in Figs. 4(a) and 4(b) is an estimate of the smallest value of k that could be measured accurately given the thickness of the films grown. This estimate was calculated by assuming that a transmission of ≤80% is required to accurately measure the imaginary index of refraction k.[3,24] Above a transmission of 80%, there is not enough light being attenuated by the film to give an accurate measurement for k.[3] Given the thickness, a minimum accurately measurable k is calculated for that thickness as a function of wavelength. A measurement below this line can be considered to be of questionable accuracy. This line was calculated using the transmission equation

$$T = \exp(-4\pi kt/\lambda), \quad (1)$$

where T is the transmission ($T = 0.8$), k is the absorption coefficient, t is the thickness of the film, and λ is the wavelength. In this manner, k was plotted as a function of wavelength for a given thickness.

It can be seen that the films of Johnson and Atreya[4] are too thin (10 μm) to accurately measure k in the weakly absorbing region from 450 to 350 cm^{-1}. The film of Trotta[23] is also too thin (14.6 μm) to accurately measure k in the weakly absorbing region. The films of Bertie *et al.*[16] varied from 0.8 to 27 μm in thickness. It can be seen from the k minimum line in Fig.

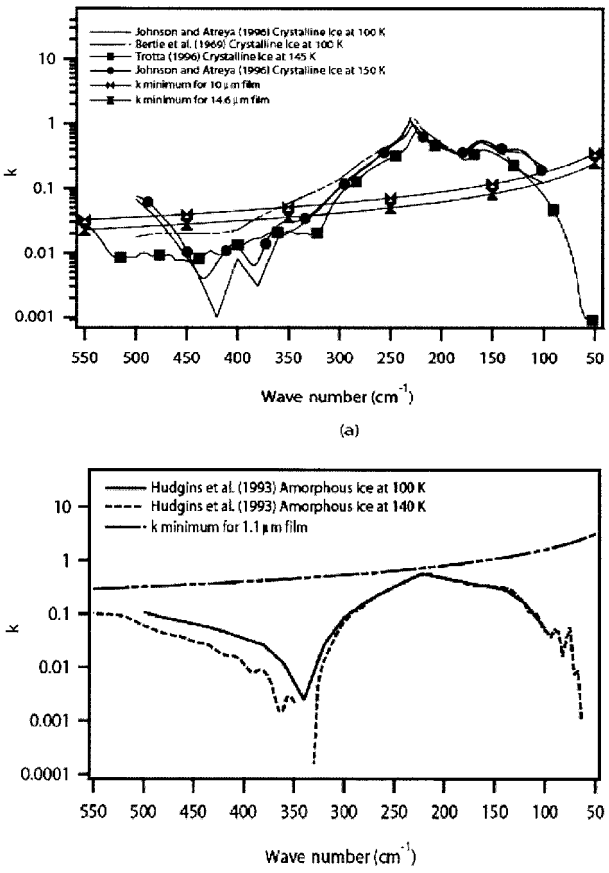

Fig. 4. (a) Comparison of the imaginary indices of refraction of Johnson and Atreya (1996),[4] Trotta (1996),[23] and Bertie *et al.* (1969)[16] at 100 K. (b) Imaginary indices of refraction of Hudgins *et al.* (1993)[21] at 100 and 140 K.

4(a) that k could be accurately measured for those films greater than 10 μm thick and that k could accurately be measured in all cases in the strongly absorbing region (300–100 cm^{-1}).

Figure 4(a) shows good agreement between Bertie *et al.*[16] and Johnson and Atreya[4] for large k values. However, Johnson and Atreya[4] were not able to determine their film thickness accurately, and they used the absorption coefficients of Bertie *et al.*[16] to fine-tune their film thickness. Hence the close agreement between these two data sets is not surprising. The 100 K samples of Bertie *et al.*[16] and Johnson and Atreya[4] were formed by cooling the film down from a higher temperature. The amorphous to crystalline phase transition is irreversible; so when cooled from a higher temperature where the crystalline phase is more stable, the sample continues to remain crystalline even at temperatures as low as 10 K.[17] The 100 K sample of Hudgins *et al.*[21] was formed by warming a film deposited initially at 10 K and is clearly amorphous. It can be seen from the k minimum line in Fig. 4(b) that the films of Hudgins *et al.* were too thin (1.1 μm) to accurately measure k over the range of wavelengths they required. As the Hudgins *et al.* data are the only set available for amorphous ice, we performed a new measurement for the optical constants of amorphous ice.

The 150 K water ice sample of Johnson and Atreya,[4] the 140 K sample of Hudgins *et al.*,[21] and the 145 K sample of Trotta[23] were prepared by warming a film formed initially by the condensation of water vapor at 77, 10, and 33 K, respectively. The 140 K water ice sample of Hudgins *et al.* appears to be amorphous, whereas those of Johnson and Atreya and Trotta are crystalline with very similar ratios of the imaginary indices at the peaks of the 225 cm^{-1} band and the 160 cm^{-1} band of 1.7 and 1.8, respectively. Trotta and Hudgins *et al.* used polyethylene substrates whereas Johnson and Atreya used a silicon substrate, and yet the results of Trotta and those of Johnson and Atreya are at least qualitatively similar (it has been determined that the substrate may affect the measurement of optical constants).[25] As described above, all these studies used films that are too thin to be useful in frequency regions of weak absorbance. On the whole, in the 150–300 cm^{-1} region the data of Johnson and Atreya[4] differ from those of Trotta[23] by ~0–60%. These discrepancies seem surprising given the similar experimental methods used. It is possible that uncertainties in film thickness in the Johnson and Atreya experiment might explain the discrepancy involving their data. So far as the fact that the Hudgins *et al.*[21] sample is amorphous even at 140 K is concerned, it has been suggested by Smith *et al.*[17] that the water molecules in direct contact with the substrate at 10 K, when the film was initially deposited, are sufficiently tightly bound that they do not gain enough energy upon warming up to above 110 K to rearrange themselves into a crystalline structure. In contrast, the water molecules in the rest of the film are able to move freely and form a crystalline structure. In this case the strength of the absorption features should be less than what they would be for a 100% crystalline water ice sample. It is also possible that the time scale for transition between amorphous and crystalline ice upon warming was too long to be measured in the Hudgins *et al.*[21] study.

The thickness of the films of Trotta[23] were measured using a He–Ne laser similar to that used in this study. However, the maximum thickness of the film was not reported. The maximum thickness of the film of Trotta was determined in the following manner. According to Trotta the growth of these films was stopped before the strongest absorbing peak was saturated (transmission of 5%). Using this value and his reported values for k, we determined a maximum thickness for the films of 14.3 μm. Therefore the films were not thick enough to accurately determine k in the weakly absorbing region.

Thick samples (that yield absorbance in the transparent spectral regions of at least $A = 0.4$) are needed to determine optical constants in the weakly absorbing regions (below 150 and 300–450 cm^{-1}) of the water ice spectrum. Furthermore, the film thickness needs to be determined accurately. Among the various experimental determinations of the far-IR optical constants of water ice mentioned in this section, only that of Trotta[23] has addressed these issues by using a He–Ne laser similar to that used in this study. Furthermore, there are no far-IR optical constants available for water ice above 150 K mostly because of the difficulty in maintaining ice films at these higher temperatures due to rapid sublimation. For cirrus clouds, optical constants will be required at a temperature at least as high as 190 K. Even for astronomical purposes it appears that optical constants of water ice in the 170–200 K range would be valuable. Hence new measurements of optical constants are necessary in the far-IR spectral region.

Warren[3] reviewed the optical constants of water ice from the ultraviolet to the microwave wavelengths. In the IR (1.4–600 μm) Warren pointed out the frequency windows where new measurements were necessary. In the near IR (1.4–2.8 μm), this need has been addressed by a number of new measurements summarized in Ref. 26. Since Warren's compilation, new measurements in the mid-IR (2.8–20 μm) are also now available.[24,27] At the time of Warren's compilation, the only optical constants available in the far IR were those of Bertie *et al.*[16] of crystalline ice at 100 K. We now have more measurements available of amorphous and crystalline ice at various temperatures, but they are in poor agreement with each other. Through experimental methods chosen to overcome the limitations encountered by the other available measurements, we hope to fulfill the need for more accurate temperature-dependent optical constants in the far IR.

4. Experiment

The apparatus used to measure IR spectra has been described in detail previously.[24,28] Briefly, polycrys-

talline and amorphous ice films up to ~140 μm thick were formed by continuously condensing water vapor on a cold 15 mm diameter silicon wafer (transparent at these frequencies, except for a band around 600 cm^{-1}) mounted in a vacuum chamber and cooled by a liquid-nitrogen cryostat. Water vapor was introduced into the chamber through leak valves positioned to backfill vapors into the chamber. With backfilled vapors, the films are expected to grow almost equally on both sides of the wafer and will not desorb in this system due to the constant influx of water vapor. The temperature of the silicon wafer was measured with several type T thermocouples. The thermocouple junctions were attached to a copper mount in close thermal contact with the silicon. The silicon wafer could be maintained at a constant temperature to within ±1 K. The measured temperatures were calibrated using the frost point of ice and the temperature-dependent vapor pressures of Marti and Mauersberger.[29]

The IR absorbances of the films were measured in transmission using a Nicolet Magna 550 Fourier-transform IR spectrometer equipped with a deuterated triglycine sulfate detector. The absorbance A is defined as the base 10 logarithm of the ratio I_0/I, where I in our experiment refers to the light intensity after passing through the vacuum-ice-substrate-ice-vacuum system, and I_0 refers to the light intensity after passing through the vacuum-substrate-vacuum system. In our experimental geometry, IR light incident normal to the surface undergoes multiple reflections within the substrate as well as within the films.[24,26,28] The theory used to extract the optical constants from the measured transmission of IR light through the film system has been described in detail previously.[24,26,28]

The determination of the optical constants is an iterative process and has been described in detail before.[24,28] The imaginary index at each frequency is determined by minimizing the squared difference between the calculated and the measured absorbance spectra for a set of films at that temperature simultaneously. Then the value of the real index at each frequency is calculated using the Kramers–Kronig relationship. Ice crystals, being uniaxial, are slightly birefringent. The crystals have been shown, however, to be isotropic within experimental uncertainties.[30,31] Hence measurements of absorbance and refraction can be made on bulk samples (polycrystalline films) and related to any crystals of ice.

5. Ice Film Thickness Determination

Recent work on the measurement of the optical constants of water ice in the near IR[26] indicated the importance of accurate film thickness measurements. Water ice films were grown over a period of several hours by condensing water vapor on the substrate cooled to the desired temperature. The film thicknesses were monitored in real time for each temperature during the 3 h film growth by two methods. First, we monitored the interference fringes of a He–Ne laser beam (λ = 632.8 nm) incident on the film at an angle of 45° to the surface normal. The He–Ne light was detected using a photodiode, and the signal was recorded as a function of time using National Instruments LabVIEW 5.1 running on a desktop PC. Second, we followed the IR signal at 500 cm^{-1} as a function of film growth. Infrared absorption spectra were recorded continuously at 4 cm^{-1} resolution at ~8 s intervals during growth of the ice films by transmitting the output of the Fourier-transform IR spectrometer normally through the ice-silicon-ice system. The absorbance at 500 cm^{-1} was then extracted from each spectrum and plotted as a function of time. This calibration was performed at each temperature. Figure 5(a) shows a typical trace of the photodiode signal (upper trace, solid curve) and the absorbance at 500 cm^{-1} (filled diamonds) plotted versus time. The calibration shown is for the spectra collected at 156 K, but the calibrations at each temperature were performed in a similar manner. At 500 cm^{-1} the absorbance is small compared to the band maximum at 225 cm^{-1}, but it is finite. This explains the positive slope with decreasing amplitude of the interference fringes and the absorbance eventually increasing linearly with time (film thickness).

The ice film thickness d can be expressed in terms of the real indices of refraction of ice (n_2) and vacuum (n_1), the wavelength (λ), and angles of incidence (θ_1) and refraction (θ_2) as follows[32]:

$$d = \frac{m\lambda}{\left(\frac{2n_2}{\cos\theta_2} - 2n_1 \sin\theta_1 \tan\theta_2\right)}, \tag{2}$$

where m is a positive integer and $m = 1$ corresponds to the first constructive interference (maximum) in the fringes. For the He–Ne beam, using λ = 632.8 nm, $\theta_1 = 45°$, $n_2 = 1.308$ (Ref. 32), and $n_1 = 1$ along with Snell's law ($n_1 \sin\theta_1 = n_2 \sin\theta_2$), we can see that the first He–Ne fringe maximum corresponds to an ice film thickness of ~0.287 μm on each side of the silicon substrate.

For the IR beam that is incident normally ($\theta_1 = 90°$) on the ice surface, Eq. (2) reduces to

$$d = \frac{m\lambda}{2n_2}. \tag{3}$$

If λ = 20 μm (500 cm^{-1}) and $n_2 = 1.429$,[23] a value for the film thickness on each side of the silicon substrate of ~70 μm is obtained at the first fringe maximum ($m = 1$). This thickness can be verified with the He–Ne fringes plotted alongside.

An expanded view of the He–Ne and IR during film growth at 156 K is shown in Fig. 5(b). To correlate the two measurements, IR spectra of those films were chosen whose absorbance at 500 cm^{-1} lay exactly between a maximum and a minimum because these points had the highest accuracy for film thickness. Typically, the He–Ne fringes deteriorated by approx-

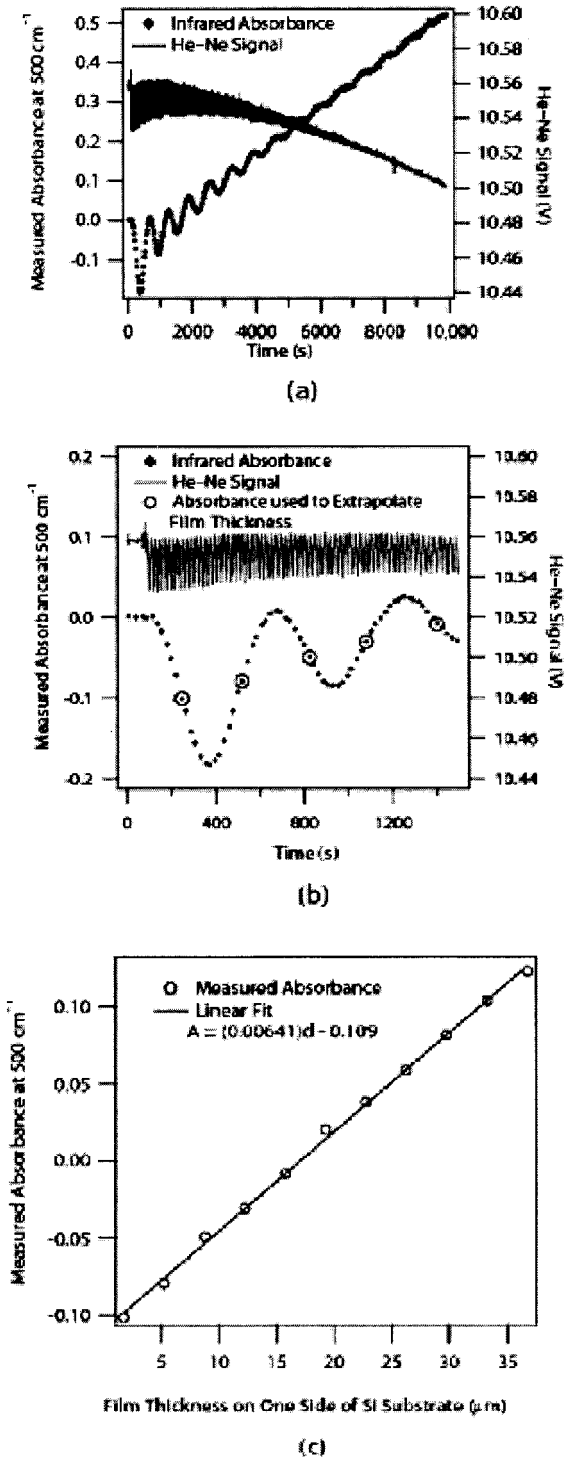

Fig. 5. (a) Typical He–Ne signal as detected by a photodiode while the water ice film is being deposited continuously for ≈3 h (solid curve) and the measured absorbance at 500 cm^{-1} (filled diamonds) plotted versus time. Spectra were recorded approximately every 8 s. Each diamond corresponds to one spectrum. (b) Expanded view of the first 1400 s. The spectra chosen for the thickness analysis are represented by open circles. The He–Ne trace is used to assign a thickness to each of those spectra. (c) The measured absorbance at 500 cm^{-1} of the chosen spectra (open circles) are plotted versus the corresponding film thickness assigned using the He–Ne interference pattern as described in the text. The solid line is a linear least-squares fit of the points to a straight line, valid only for thickness greater than 1.75 μm.

imately the fifth IR fringe (~70 μm total film thickness, counting both sides of the silicon substrate) and were no longer useful for thickness calibration beyond that point. Thus the IR absorbance at 500 cm^{-1} was calibrated to the He–Ne film thickness, and the calibration was used to determine the film thickness for all films. Figure 5(c) is a plot of the absorbance at 500 cm^{-1} of the chosen spectra versus the associated He–Ne film thickness (circles), along with a straight-line fit to the data (solid line). An excellent correlation between the two measurements was found. Thus the IR absorbance at 500 cm^{-1} was calibrated to the He–Ne signal and that calibration line was used to determine the thickness of the film as it grew over a 3 h period.

At higher thickness, there is a loss of coherence in the film. This results in a decrease in the amplitude of the oscillation interference of the He–Ne signal and of the IR signal. This does not affect the measurement of thickness at higher values because of the straight-line fit through the plot in Fig. 5(c).

6. Optical Constant Calculation

For the determination of the imaginary index of refraction k in the 50–650 cm^{-1} region, the ice films were divided into three groups. The thin group consisting of films less than 11 μm thick was used for the determination of k in the regions of relatively strong absorbance. The thick group consisting of films ~41–140 μm thick was used for the determination of k in the regions of relatively weakest absorbance, and the intermediate group was used to determine k at the remaining frequencies. Each group consists of a minimum of three films that are fit simultaneously to determine k and n.

As mentioned above, the determination of the optical constants is an iterative process that involves the following steps.[24,28] First we input the film thickness and an initial estimate of the optical constants from Trotta[23] at 145 K. Optical constants for the silicon substrate were taken from the *Handbook of Optical Constants of Solids*.[33]

Then the k values are determined by minimizing the mean-square difference between the measured and calculated transmission for all the films chosen in a given run. The imaginary index is adjusted until the mean difference is less than 0.005 absorbance units, or until the mean difference stops declining. Using these adjusted values of k over the entire wavelength range, the real indices of refraction are calculated using the Kramers–Kronig relationship.[24,28] Table 2 summarizes the imaginary indices available in the literature that were used to extend the imaginary indices beyond the range of our present measurements for the Kramers–Kronig integration. The integration is performed from approximately 1.9 to 185,806 cm^{-1}. Below 52 cm^{-1} and above 6997 cm^{-1} the imaginary indices are assumed to remain constant at the values corresponding to 52 and 6997 cm^{-1}, respectively. Also listed in Table 2 are the anchor points[24,26,28,34] for the Kramers–Kronig integration, chosen to be the

Table 2. Imaginary Indices of Refraction Used for the Calculation of the Real Indices Using the Kramers–Kronig Integration[a]

	Approximate Frequency Range (cm^{-1})				
Temperature (K)	52–500	500–800	800–3700	3700–7000	n at 15, 823 cm^{-1}
106	Trotta (1996), 145 K1	Toon *et al.* (1994), 166 K	Clapp *et al.* (1995), 130 K	Rajaram *et al.* (2001), 170 K	1.28
116	Trotta (1996), 145 K	Toon *et al.* (1994), 166 K	Clapp *et al.* (1995), 130 K	Rajaram *et al.* (2001), 170 K	1.29
126	Trotta (1996), 145 K	Toon *et al.* (1994), 166 K	Clapp *et al.* (1995), 130 K1	Rajaram *et al.* (2001), 170 K	1.30
136	Trotta (1996), 145 K	Toon *et al.* (1994), 166 K	Clapp *et al.* (1995), 130 K	Rajaram *et al.* (2001), 170 K	1.310459
146	Trotta (1996), 145 K	Toon *et al.* (1994), 166 K	Clapp *et al.* (1995), 150 K	Rajaram *et al.* (2001), 170 K	1.310303
156	Trotta (1996), 145 K	Toon *et al.* (1994), 166 K	Clapp *et al.* (1995), 160 K	Rajaram *et al.* (2001), 170 K	1.310110
166	Trotta (1996), 145 K	Toon *et al.* (1994), 166 K	Clapp *et al.* (1995), 170 K	Rajaram *et al.* (2001), 170 K	1.309880
176	Trotta (1996), 145 K	Toon *et al.* (1994), 166 K	Clapp *et al.* (1995), 180 K	Rajaram *et al.* (2001), 170 K	1.309615

[a]The last column has the temperature-dependent real index of refraction at 15, 823 cm^{-1} used as the anchor point for the Kramers–Kronig analysis. For $T = 136$ K and higher, these were calculated using the Lorentz–Lorenz equation; see Rajaram *et al.* (2001)[26] for details. For $T = 126$ and lower, these values are measured values from Berland *et al.* (1995).[34] The values of Trotta (1996)[23] were used as the starting point for the iteration in the far IR in this study, while those of Toon *et al.* (1994),[24] Clapp *et al.* (1995),[27] and Rajaram *et al.* (2001)[26] were used in the mid-IR and near IR.

temperature-dependent real index of refraction at the frequency 15, 823 cm^{-1}. After the real indices are calculated, the whole cycle repeats. These overall iterations continue until the changes in the real and imaginary index from one set of iterations to the next are less than 1%. Figure 6 shows typical fits between the measured and the calculated absorbance spectra that we have been able to achieve.

At each temperature three iterations were made, one each for the thin, intermediate, and thick film groups. The final values for k were obtained by splicing together the results for the three groups as summarized in Table 3. Rather than splice the real indices from the three groups, the final values for n were simply recalculated using the Kramers–Kronig integration and our final k values in the 50–650 cm^{-1} region. Because we explicitly account for the oscillations in the spectra with our technique, it is not necessary to perform any other baseline corrections to our raw spectra.

7. Results and Discussion

A. Amorphous to Crystalline Ice Transition

The real and imaginary indices of refraction from 106 to 176 K in the 50–650 cm^{-1} spectral range determined in this study are shown in Figs. 7(a) and 7(b), respectively, and are listed in Tables 4 and 5. It can be seen from the k minimum calculation shown in Fig. 7(b) that our films are thick enough (thickest films $\sim$140 μm) to accurately measure k over the entire spectrum.

It is clear that there is a transition from amorphous to crystalline phase between deposition at 126 and 136 K as determined by the appearance of the 160 cm^{-1} band and by the dramatic increase in the strength of the 225 cm^{-1} band at and above 136 K. Our results also show that the amorphous to crystalline phase transition is accompanied by a shift in the frequency of the TO band from around 218 cm^{-1} in the amorphous phase to $\approx$225 cm^{-1} for the crystalline phase. The transition was observed by Smith *et al.*[17] using a polyethylene substrate between 110 and 120 K. The far-IR spectrum of water ice has also been investigated using other substrates by Maldoni *et al.*[18] Using a polyethylene substrate coated with an amorphous silicate film, they observed the transition from amorphous ice to crystalline ice at 130 K. Moore and Hudson[19] observed ice crystallization as low as 20 K using amorphous silicate smokes on an aluminum substrate. This substrate revealed smoke grains between 5 and 10 nm, while that used by Maldoni *et al.*[18] was seen under a scanning electron microscope to be a smooth homogeneous surface. It is clear that the transition temperature depends not only on the

Table 3. Groups of Films Used to Obtain the Imaginary Index of Refraction in the 50–650 cm^{-1} Region[a]

Approximate Frequency Range (cm^{-1})	Group of Films
52–144	Thick
148–198	Intermediate
202–248	Thin
252–302	Intermediate
306–545	Thick
549–650	Intermediate

[a]The thin group refers to films $\leq$ 11 μm thick. The intermediate group consists of films 12–41 μm thick, and the thick group consists of films 41–140 μm thick.

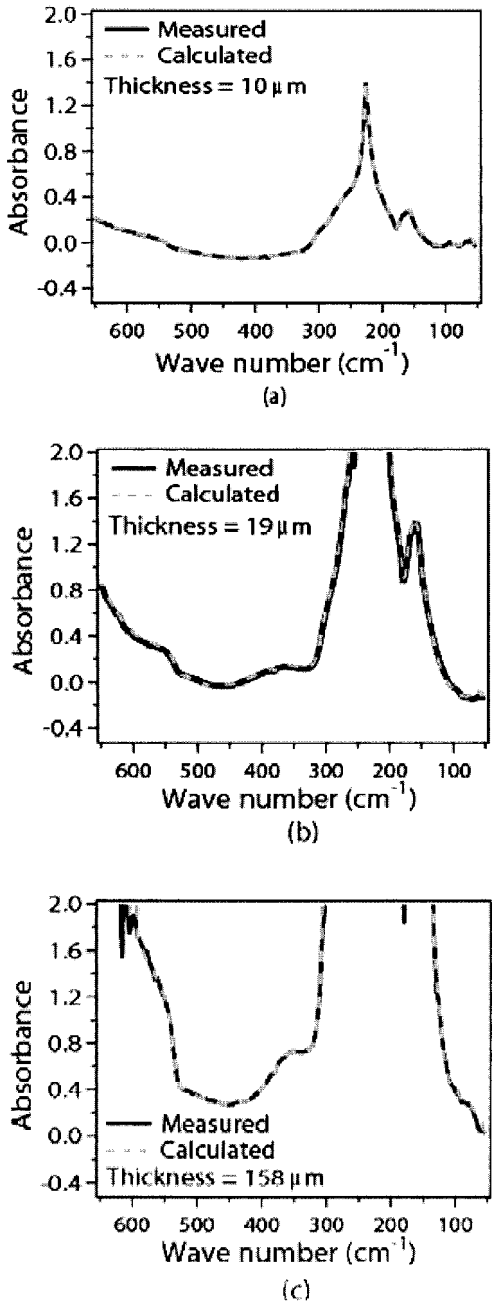

Fig. 6. Typical fits between the calculated and measured absorbance spectra that we were able to obtain. Examples were chosen to span the (a) thin, (b) intermediate, and (c) thick film groups.

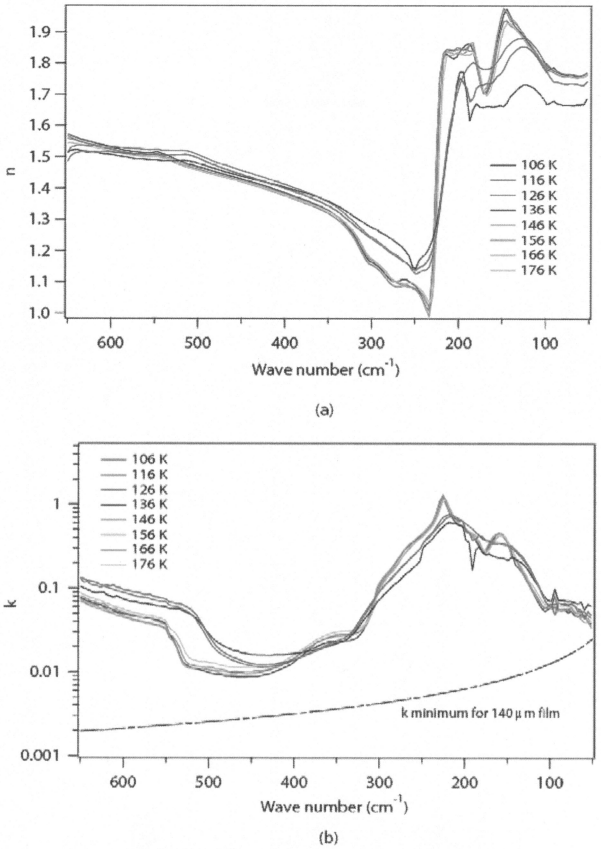

Fig. 7. (a) Temperature-dependent real indices of refraction n that were determined in this study. (b) Temperature-dependent imaginary indices of refraction k that were determined in this study.

material of the substrate but also on the surface roughness. Our silicon substrate is an optical quality crystalline substrate that might explain the higher transition temperature observed in this study than in some of the other studies mentioned above.

Table 6 summarizes the band shifts that we obtained during the amorphous to crystalline transition using absorbance spectra of films around 5.3 μm thick at the various temperatures. Also shown is the ratio of the peak heights (225 cm^{-1} TO band to the 160 cm^{-1} longitudinal acoustic band) for the spectra at and above 136 K (crystalline phase). This ratio has been shown to depend on the substrate and on thermal history of the ice film.[17,18] For example, this ratio has been found to be larger for films formed by direct deposition at a particular temperature than for films formed by initial deposition at a low temperature followed by warming to higher temperatures. The far-IR bands discussed here are much more sensitive to phase change than the bands in the mid-IR.[18] This is most likely due to the fact that, whereas the bands in the mid-IR are intramolecular in origin, the lattice modes observed in the far IR are intermolecular in origin.

B. Cubic to Hexagonal Ice Transition

Although cubic ice (ice I_c) and hexagonal ice (ice I_h) have been shown to be indistinguishable in the mid-IR,[16] it has been suggested that there is a slight difference in the far IR.[22] This difference is mainly in the peak at 160 cm^{-1}, which is a single peak in ice I_c, but appears as a doublet in ice I_h, with the addition of a peak at around 170 cm^{-1}. Although it is difficult to distinguish within the resolution of this experiment, we do note a very slight shoulder at ~167 cm^{-1} for some of our spectra. This shoulder is not present in the spectra of films grown at 136 K, indicating that these films are likely composed of crystalline ice I_c.

Table 4. Measured Optical Constants for Water Ice from 106 to 136 K

Frequency (cm^{-1})	106 K		116 K		126 K		136 K	
	n	k	n	k	n	k	n	k
52.069	1.713	0.0628	1.772	0.0471	1.771	0.0447	1.768	0.0381
55.927	1.695	0.0648	1.759	0.0529	1.763	0.0486	1.761	0.0449
59.785	1.693	0.0568	1.759	0.0437	1.759	0.0531	1.757	0.0469
63.643	1.693	0.0695	1.764	0.0549	1.759	0.0529	1.756	0.0483
67.501	1.689	0.0666	1.764	0.0572	1.763	0.0540	1.757	0.0468
71.360	1.690	0.0689	1.765	0.0625	1.765	0.0620	1.761	0.0480
75.218	1.689	0.0713	1.764	0.0670	1.763	0.0658	1.763	0.0538
79.076	1.689	0.0708	1.766	0.0630	1.764	0.0646	1.765	0.0516
82.934	1.691	0.0721	1.769	0.0674	1.767	0.0642	1.769	0.0548
86.792	1.693	0.0727	1.773	0.0664	1.772	0.0656	1.775	0.0539
90.650	1.695	0.0738	1.777	0.0686	1.776	0.0678	1.787	0.0548
94.508	1.698	0.0727	1.783	0.0664	1.783	0.0651	1.782	0.0852
98.366	1.705	0.0716	1.794	0.0641	1.793	0.0653	1.776	0.0604
102.224	1.716	0.0722	1.811	0.0627	1.808	0.0633	1.789	0.0570
106.082	1.728	0.0802	1.831	0.0730	1.827	0.0720	1.804	0.0534
109.940	1.738	0.0908	1.849	0.0900	1.844	0.0876	1.822	0.0585
113.798	1.747	0.106	1.862	0.110	1.858	0.107	1.840	0.0675
117.656	1.752	0.123	1.874	0.131	1.870	0.127	1.856	0.0805
121.514	1.756	0.141	1.882	0.159	1.879	0.152	1.872	0.0950
125.372	1.754	0.164	1.885	0.187	1.881	0.181	1.886	0.113
129.230	1.744	0.184	1.884	0.213	1.880	0.203	1.900	0.133
133.088	1.734	0.195	1.877	0.246	1.878	0.229	1.911	0.157
136.946	1.723	0.207	1.866	0.264	1.873	0.253	1.923	0.175
140.805	1.712	0.211	1.855	0.289	1.864	0.278	1.951	0.191
144.663	1.705	0.215	1.840	0.306	1.854	0.299	1.975	0.261
148.521	1.700	0.219	1.824	0.322	1.839	0.323	1.957	0.346
152.379	1.695	0.223	1.811	0.328	1.820	0.337	1.916	0.389
156.237	1.692	0.228	1.800	0.339	1.804	0.345	1.869	0.433
160.095	1.689	0.233	1.792	0.344	1.791	0.351	1.800	0.460
163.953	1.688	0.236	1.788	0.350	1.783	0.354	1.733	0.433
167.811	1.687	0.244	1.787	0.363	1.781	0.358	1.703	0.370
171.669	1.687	0.249	1.786	0.375	1.781	0.367	1.706	0.326
175.527	1.691	0.253	1.786	0.394	1.784	0.376	1.738	0.280
179.385	1.695	0.268	1.785	0.414	1.796	0.390	1.793	0.276
183.243	1.697	0.278	1.787	0.436	1.803	0.431	1.840	0.316
187.101	1.708	0.287	1.784	0.478	1.796	0.472	1.862	0.374
190.959	1.719	0.318	1.769	0.519	1.782	0.512	1.861	0.427
194.817	1.727	0.349	1.745	0.561	1.761	0.553	1.852	0.469
198.675	1.725	0.404	1.713	0.603	1.733	0.593	1.838	0.511
202.533	1.704	0.460	1.667	0.645	1.697	0.634	1.821	0.545
206.391	1.661	0.519	1.615	0.670	1.652	0.675	1.815	0.566
210.249	1.603	0.553	1.560	0.695	1.597	0.712	1.822	0.612
214.108	1.534	0.587	1.491	0.720	1.524	0.749	1.829	0.679
217.966	1.454	0.586	1.408	0.724	1.435	0.761	1.828	0.791
221.824	1.380	0.564	1.320	0.701	1.342	0.747	1.758	0.993
225.682	1.324	0.513	1.254	0.636	1.253	0.705	1.498	1.23
229.540	1.288	0.469	1.213	0.581	1.185	0.631	1.160	1.12
233.398	1.263	0.426	1.183	0.524	1.148	0.549	1.010	0.808
237.256	1.248	0.385	1.166	0.471	1.139	0.478	1.020	0.638
241.114	1.239	0.351	1.158	0.424	1.138	0.435	1.047	0.550
244.972	1.230	0.325	1.153	0.388	1.131	0.397	1.070	0.485
248.830	1.217	0.299	1.145	0.352	1.126	0.348	1.088	0.447
252.688	1.208	0.258	1.148	0.299	1.135	0.300	1.095	0.415
256.546	1.213	0.217	1.162	0.272	1.152	0.269	1.101	0.378
260.404	1.225	0.190	1.171	0.248	1.163	0.251	1.108	0.355
264.262	1.236	0.171	1.178	0.227	1.170	0.229	1.108	0.333
268.120	1.247	0.151	1.186	0.205	1.179	0.206	1.104	0.309
271.978	1.258	0.139	1.195	0.188	1.187	0.192	1.101	0.276
275.836	1.267	0.127	1.203	0.172	1.194	0.174	1.104	0.244

Table 4. Continued

Frequency (cm^{-1})	106 K		116 K		126 K		136 K	
	n	k	n	k	n	k	n	k
279.694	1.275	0.117	1.210	0.156	1.201	0.158	1.111	0.213
283.552	1.282	0.108	1.218	0.140	1.210	0.141	1.123	0.184
287.411	1.288	0.0991	1.227	0.128	1.219	0.129	1.137	0.164
291.269	1.294	0.0900	1.235	0.117	1.227	0.116	1.148	0.148
295.127	1.301	0.0827	1.243	0.105	1.235	0.106	1.156	0.132
298.985	1.307	0.0753	1.250	0.0953	1.242	0.0954	1.163	0.116
302.843	1.312	0.0688	1.257	0.0849	1.248	0.0849	1.168	0.0993
306.701	1.318	0.0596	1.265	0.0738	1.257	0.0703	1.181	0.0660
310.559	1.325	0.0534	1.274	0.0648	1.268	0.0620	1.202	0.0519
314.417	1.331	0.0477	1.283	0.0568	1.278	0.0536	1.221	0.0400
318.275	1.338	0.0424	1.292	0.0498	1.288	0.0462	1.240	0.0322
322.133	1.345	0.0374	1.301	0.0431	1.298	0.0402	1.257	0.0281
325.991	1.352	0.0332	1.310	0.0372	1.307	0.0349	1.271	0.0258
329.849	1.359	0.0297	1.320	0.0327	1.317	0.0312	1.284	0.0246
333.707	1.366	0.0272	1.329	0.0294	1.326	0.0285	1.295	0.0238
337.565	1.372	0.0252	1.337	0.0270	1.335	0.0267	1.305	0.0235
341.423	1.378	0.0241	1.345	0.0254	1.342	0.0253	1.313	0.0234
345.281	1.383	0.0232	1.352	0.0242	1.349	0.0244	1.321	0.0234
349.139	1.388	0.0223	1.358	0.0232	1.355	0.0235	1.328	0.0235
352.997	1.393	0.0217	1.364	0.0224	1.361	0.0227	1.334	0.0232
356.855	1.397	0.0212	1.370	0.0215	1.366	0.0220	1.339	0.0229
360.714	1.401	0.0206	1.375	0.0208	1.371	0.0213	1.344	0.0225
364.572	1.405	0.0200	1.379	0.0199	1.376	0.0204	1.349	0.0220
368.430	1.409	0.0196	1.384	0.0192	1.380	0.0196	1.353	0.0213
372.288	1.412	0.0192	1.388	0.0183	1.384	0.0188	1.358	0.0204
376.146	1.415	0.0187	1.393	0.0177	1.389	0.0180	1.362	0.0196
380.004	1.419	0.0184	1.397	0.0170	1.393	0.0173	1.366	0.0192
383.862	1.422	0.0180	1.401	0.0163	1.397	0.0165	1.369	0.0177
387.720	1.425	0.0177	1.405	0.0157	1.400	0.0159	1.373	0.0166
391.578	1.428	0.0174	1.409	0.0152	1.404	0.0152	1.377	0.0154
395.436	1.431	0.0171	1.412	0.0147	1.408	0.0145	1.381	0.0143
399.294	1.433	0.0169	1.416	0.0142	1.412	0.0139	1.385	0.0133
403.152	1.436	0.0167	1.420	0.0138	1.415	0.0135	1.389	0.0125
407.010	1.439	0.0165	1.423	0.0135	1.419	0.0129	1.393	0.0119
410.868	1.442	0.0163	1.427	0.0131	1.422	0.0126	1.396	0.0113
414.726	1.444	0.0163	1.430	0.0129	1.426	0.0123	1.400	0.0109
418.584	1.447	0.0162	1.434	0.0127	1.429	0.0120	1.404	0.0105
422.442	1.450	0.0162	1.437	0.0126	1.433	0.0119	1.407	0.0101
426.300	1.452	0.0161	1.441	0.0125	1.436	0.0117	1.410	0.00969
430.158	1.455	0.0161	1.444	0.0124	1.440	0.0116	1.414	0.00945
434.017	1.457	0.0161	1.447	0.0123	1.443	0.0116	1.417	0.00923
437.875	1.460	0.0161	1.451	0.0124	1.446	0.0115	1.420	0.00904
441.733	1.462	0.0161	1.454	0.0123	1.450	0.0116	1.423	0.00891
445.591	1.465	0.0163	1.458	0.0127	1.453	0.0117	1.426	0.00882
449.449	1.468	0.0164	1.461	0.0127	1.456	0.0119	1.429	0.00880
453.307	1.471	0.0165	1.464	0.0130	1.459	0.0121	1.432	0.00879
457.165	1.473	0.0168	1.468	0.0133	1.463	0.0123	1.435	0.00871
461.023	1.476	0.0170	1.471	0.0137	1.466	0.0126	1.438	0.00873
464.881	1.479	0.0177	1.475	0.0142	1.470	0.0130	1.441	0.00872
468.739	1.482	0.0180	1.479	0.0148	1.473	0.0135	1.444	0.00878
472.597	1.485	0.0186	1.482	0.0152	1.477	0.0138	1.447	0.00886
476.455	1.488	0.0194	1.486	0.0158	1.480	0.0145	1.450	0.00894
480.313	1.491	0.0200	1.490	0.0167	1.484	0.0152	1.453	0.00892
484.171	1.494	0.0212	1.495	0.0179	1.488	0.0160	1.456	0.00924
488.029	1.498	0.0224	1.499	0.0193	1.493	0.0172	1.459	0.00930
491.887	1.501	0.0239	1.504	0.0211	1.497	0.0186	1.462	0.00939
495.745	1.505	0.0257	1.509	0.0237	1.502	0.0207	1.465	0.00957
499.603	1.509	0.0285	1.514	0.0271	1.507	0.0235	1.468	0.00981
503.462	1.512	0.0317	1.518	0.0315	1.511	0.0273	1.471	0.0101

Table 4. Continued

Frequency (cm^{-1})	106 K		116 K		126 K		136 K	
	n	k	n	k	n	k	n	k
507.320	1.514	0.0359	1.522	0.0369	1.515	0.0321	1.474	0.0104
511.178	1.516	0.0402	1.524	0.0429	1.518	0.0370	1.477	0.0107
515.036	1.517	0.0443	1.525	0.0489	1.519	0.0425	1.481	0.0109
518.894	1.517	0.0479	1.525	0.0536	1.520	0.0473	1.484	0.0111
522.752	1.516	0.0501	1.524	0.0575	1.519	0.0512	1.489	0.0117
526.610	1.516	0.0522	1.524	0.0601	1.519	0.0533	1.493	0.0123
530.468	1.516	0.0541	1.524	0.0634	1.519	0.0557	1.498	0.0134
534.326	1.516	0.0561	1.523	0.0648	1.520	0.0585	1.504	0.0160
538.184	1.515	0.0563	1.523	0.0655	1.520	0.0600	1.508	0.0209
542.042	1.516	0.0571	1.525	0.0670	1.521	0.0608	1.511	0.0249
545.900	1.517	0.0574	1.528	0.0675	1.523	0.0626	1.515	0.0281
549.758	1.518	0.0594	1.528	0.0758	1.523	0.0678	1.515	0.0373
553.616	1.518	0.0607	1.527	0.0768	1.522	0.0696	1.513	0.0396
557.474	1.519	0.0611	1.526	0.0787	1.522	0.0701	1.513	0.0408
561.332	1.520	0.0615	1.526	0.0800	1.523	0.0715	1.513	0.0422
565.190	1.521	0.0630	1.527	0.0814	1.524	0.0728	1.514	0.0427
569.048	1.522	0.0636	1.527	0.0850	1.525	0.0750	1.515	0.0440
572.906	1.523	0.0642	1.526	0.0848	1.525	0.0769	1.516	0.0446
576.765	1.525	0.0650	1.528	0.0858	1.526	0.0777	1.517	0.0448
580.623	1.526	0.0657	1.529	0.0883	1.527	0.0784	1.519	0.0453
584.481	1.528	0.0669	1.529	0.0901	1.528	0.0803	1.521	0.0459
588.339	1.530	0.0684	1.530	0.0914	1.530	0.0821	1.523	0.0467
592.197	1.532	0.0691	1.530	0.0934	1.531	0.0842	1.526	0.0475
596.055	1.534	0.0712	1.531	0.0951	1.532	0.0863	1.528	0.0485
599.913	1.536	0.0728	1.533	0.0954	1.533	0.0878	1.531	0.0495
603.771	1.538	0.0759	1.534	0.101	1.534	0.0914	1.534	0.0508
607.629	1.537	0.0798	1.534	0.103	1.535	0.0924	1.537	0.0521
611.487	1.539	0.0769	1.531	0.109	1.537	0.0960	1.540	0.0538
615.345	1.542	0.0798	1.531	0.105	1.537	0.0992	1.542	0.0575
619.203	1.544	0.0824	1.531	0.110	1.536	0.103	1.545	0.0579
623.061	1.544	0.0887	1.531	0.108	1.534	0.105	1.548	0.0598
626.919	1.542	0.0885	1.533	0.110	1.535	0.102	1.550	0.0627
630.777	1.544	0.0869	1.534	0.115	1.536	0.107	1.553	0.0635
634.635	1.547	0.0871	1.533	0.119	1.536	0.108	1.556	0.0656
638.493	1.550	0.0923	1.530	0.122	1.537	0.111	1.560	0.0673
642.351	1.550	0.0959	1.527	0.125	1.534	0.119	1.564	0.0698
646.209	1.549	0.0992	1.520	0.129	1.530	0.117	1.568	0.0730
650.067	1.542	0.104	1.501	0.133	1.513	0.131	1.572	0.0761

This shoulder is most strongly present in the films grown at 176 K, indicating that these films are likely composed of crystalline I_h. The spectra at 146, 156, and 166 K also show some indication of the shoulder, indicating that they are at least partially composed of I_h or some mixture of I_h and I_c.

C. Comparison of Optical Constants for Amorphous Ice

Comparison of our optical constants at 106 K with the 100 K results of Hudgins *et al.*[21] is presented in Figs. 8 and 9. The 100 K sample of Hudgins *et al.* was formed by warming a film deposited initially at 10 K (series I of Smith *et al.*[17]), and our 110 K sample was prepared by direct deposition at that temperature (series II of Smith *et al.*[17]). Both of these samples are clearly amorphous. Smith *et al.* have shown that spectra of amorphous ice directly deposited at 100 K and that of ice warmed from a cooler temperature are similar. In particular, the peak strength of the TO band is similar in both cases but the features in the spectra of the directly deposited films are broader. The real indices of refraction between our data and that of Hudgins *et al.*[21] are in agreement to within $\pm 7\%$. The differences in the imaginary indices in all regions of the spectrum are greater than in the real indices. Above and below the 150–300 cm^{-1} region the differences are very large (up to $\sim 300\%$) because the samples of Hudgins *et al.* were too thin to accurately measure k in these regions of little absorbance. In the absorbing region (150–300 cm^{-1}) the differences are smaller, varying between -35 and $+30\%$.

D. Comparison of Optical Constants for Crystalline Ice

Our 146 K optical constants are compared with those of Trotta[23] at 145 K and those of Johnson and Atreya[4]

Table 5. Measured Optical Constants for Water Ice from 146 to 176 K

Frequency (cm^{-1})	146 K		156 K		166 K		176 K	
	n	k	n	k	n	k	n	k
52.069	1.766	0.0406	1.769	0.0360	1.764	0.0339	1.764	0.0402
55.927	1.759	0.0392	1.765	0.0395	1.758	0.0429	1.759	0.0431
59.785	1.759	0.0395	1.761	0.0500	1.756	0.0436	1.756	0.0539
63.643	1.762	0.0427	1.760	0.0448	1.756	0.0499	1.752	0.0518
67.501	1.765	0.0470	1.763	0.0518	1.755	0.0507	1.755	0.0502
71.360	1.766	0.0523	1.763	0.0536	1.758	0.0511	1.760	0.0541
75.218	1.766	0.0538	1.762	0.0583	1.759	0.0590	1.761	0.0613
79.076	1.767	0.0555	1.763	0.0550	1.758	0.0575	1.761	0.0612
82.934	1.769	0.0548	1.767	0.0552	1.761	0.0575	1.764	0.0620
86.792	1.774	0.0542	1.771	0.0548	1.765	0.0565	1.769	0.0619
90.650	1.779	0.0546	1.779	0.0544	1.771	0.0583	1.780	0.0625
94.508	1.788	0.0498	1.784	0.0620	1.777	0.0586	1.777	0.0898
98.366	1.799	0.0581	1.789	0.0573	1.784	0.0600	1.773	0.0671
102.224	1.804	0.0629	1.798	0.0603	1.792	0.0613	1.787	0.0658
106.082	1.814	0.0594	1.810	0.0575	1.804	0.0590	1.802	0.0645
109.940	1.830	0.0620	1.827	0.0607	1.821	0.0645	1.819	0.0731
113.798	1.847	0.0713	1.844	0.0708	1.837	0.0751	1.835	0.0836
117.656	1.863	0.0825	1.860	0.0823	1.851	0.0881	1.849	0.0987
121.514	1.878	0.0969	1.876	0.0955	1.866	0.101	1.861	0.113
125.372	1.894	0.113	1.892	0.115	1.881	0.120	1.877	0.126
129.230	1.908	0.136	1.908	0.132	1.894	0.143	1.892	0.152
133.088	1.925	0.152	1.923	0.163	1.907	0.164	1.903	0.176
136.946	1.938	0.193	1.932	0.192	1.914	0.201	1.914	0.205
140.805	1.942	0.219	1.936	0.224	1.919	0.222	1.928	0.237
144.663	1.966	0.237	1.961	0.231	1.937	0.251	1.929	0.298
148.521	1.972	0.329	1.977	0.323	1.934	0.330	1.910	0.351
152.379	1.937	0.388	1.942	0.403	1.900	0.380	1.867	0.410
156.237	1.888	0.433	1.877	0.455	1.845	0.431	1.808	0.425
160.095	1.826	0.458	1.803	0.467	1.779	0.429	1.753	0.425
163.953	1.767	0.443	1.746	0.432	1.735	0.396	1.712	0.386
167.811	1.725	0.413	1.713	0.398	1.710	0.365	1.696	0.346
171.669	1.709	0.354	1.703	0.342	1.710	0.310	1.713	0.291
175.527	1.737	0.297	1.738	0.281	1.754	0.265	1.764	0.270
179.385	1.807	0.272	1.811	0.270	1.817	0.283	1.817	0.301
183.243	1.867	0.344	1.858	0.350	1.842	0.358	1.834	0.370
187.101	1.863	0.432	1.859	0.405	1.840	0.385	1.828	0.401
190.959	1.839	0.455	1.849	0.445	1.844	0.419	1.827	0.431
194.817	1.830	0.478	1.844	0.468	1.843	0.456	1.827	0.462
198.675	1.829	0.500	1.846	0.504	1.849	0.482	1.835	0.492
202.533	1.831	0.537	1.844	0.549	1.850	0.547	1.835	0.557
206.391	1.832	0.578	1.840	0.593	1.842	0.588	1.826	0.603
210.249	1.834	0.633	1.840	0.647	1.845	0.647	1.828	0.661
214.108	1.836	0.705	1.845	0.722	1.845	0.740	1.823	0.772
217.966	1.827	0.820	1.834	0.856	1.813	0.894	1.762	0.942
221.824	1.756	1.01	1.739	1.08	1.656	1.13	1.543	1.17
225.682	1.485	1.27	1.405	1.34	1.316	1.25	1.226	1.12
229.540	1.141	1.13	1.067	1.05	1.057	0.937	1.051	0.846
233.398	1.004	0.813	0.990	0.769	1.019	0.719	1.033	0.672
237.256	1.020	0.649	1.014	0.630	1.039	0.601	1.053	0.567
241.114	1.046	0.571	1.041	0.549	1.061	0.529	1.071	0.510
244.972	1.063	0.509	1.063	0.489	1.074	0.485	1.080	0.463
248.830	1.077	0.464	1.080	0.454	1.076	0.445	1.091	0.417
252.688	1.085	0.431	1.083	0.429	1.080	0.399	1.098	0.394
256.546	1.086	0.400	1.083	0.390	1.088	0.365	1.098	0.363
260.404	1.091	0.363	1.087	0.360	1.094	0.336	1.095	0.340
264.262	1.092	0.346	1.087	0.337	1.095	0.312	1.095	0.298
268.120	1.087	0.315	1.084	0.306	1.095	0.280	1.101	0.274
271.978	1.087	0.279	1.084	0.273	1.100	0.248	1.102	0.249
275.836	1.092	0.250	1.090	0.240	1.108	0.219	1.106	0.214

Table 5. Continued

Frequency (cm^{-1})	146 K		156 K		166 K		176 K	
	n	k	n	k	n	k	n	k
279.694	1.099	0.218	1.099	0.208	1.119	0.191	1.119	0.184
283.552	1.112	0.190	1.113	0.181	1.133	0.170	1.134	0.163
287.411	1.126	0.168	1.127	0.163	1.145	0.153	1.146	0.148
291.269	1.138	0.153	1.139	0.147	1.155	0.138	1.156	0.133
295.127	1.147	0.138	1.147	0.132	1.163	0.122	1.164	0.116
298.985	1.153	0.122	1.154	0.116	1.170	0.107	1.173	0.100
302.843	1.158	0.104	1.159	0.0982	1.175	0.0888	1.182	0.0821
306.701	1.170	0.0732	1.172	0.0653	1.190	0.0584	1.197	0.0573
310.559	1.190	0.0562	1.195	0.0495	1.213	0.0455	1.218	0.0456
314.417	1.210	0.0423	1.216	0.0391	1.233	0.0374	1.237	0.0393
318.275	1.230	0.0348	1.235	0.0335	1.250	0.0334	1.253	0.0357
322.133	1.247	0.0311	1.251	0.0310	1.265	0.0313	1.267	0.0337
325.991	1.262	0.0293	1.265	0.0296	1.278	0.0300	1.278	0.0325
329.849	1.275	0.0284	1.277	0.0286	1.288	0.0294	1.289	0.0316
333.707	1.286	0.0276	1.287	0.0279	1.298	0.0288	1.298	0.0312
337.565	1.295	0.0272	1.296	0.0274	1.307	0.0286	1.306	0.0309
341.423	1.304	0.0270	1.305	0.0273	1.314	0.0286	1.313	0.0310
345.281	1.311	0.0268	1.312	0.0272	1.320	0.0283	1.319	0.0308
349.139	1.318	0.0267	1.318	0.0270	1.326	0.0279	1.325	0.0303
352.997	1.324	0.0264	1.324	0.0267	1.332	0.0275	1.330	0.0298
356.855	1.330	0.0259	1.329	0.0261	1.337	0.0268	1.334	0.0290
360.714	1.335	0.0254	1.334	0.0254	1.341	0.0259	1.339	0.0280
364.572	1.340	0.0247	1.339	0.0245	1.346	0.0249	1.343	0.0269
368.430	1.344	0.0237	1.343	0.0236	1.350	0.0239	1.347	0.0257
372.288	1.348	0.0229	1.348	0.0227	1.354	0.0229	1.351	0.0246
376.146	1.352	0.0219	1.351	0.0216	1.358	0.0218	1.355	0.0233
380.004	1.357	0.0204	1.356	0.0194	1.362	0.0205	1.359	0.0220
383.862	1.361	0.0198	1.360	0.0192	1.366	0.0194	1.363	0.0207
387.720	1.364	0.0185	1.364	0.0181	1.370	0.0181	1.366	0.0195
391.578	1.368	0.0172	1.368	0.0168	1.373	0.0169	1.370	0.0184
395.436	1.372	0.0159	1.372	0.0157	1.377	0.0158	1.374	0.0172
399.294	1.376	0.0147	1.376	0.0147	1.381	0.0148	1.378	0.0162
403.152	1.380	0.0137	1.379	0.0139	1.385	0.0141	1.381	0.0153
407.010	1.384	0.0130	1.383	0.0133	1.389	0.0135	1.385	0.0144
410.868	1.388	0.0124	1.387	0.0127	1.392	0.0128	1.389	0.0136
414.726	1.392	0.0120	1.390	0.0120	1.396	0.0122	1.392	0.0129
418.584	1.395	0.0116	1.394	0.0116	1.399	0.0118	1.396	0.0125
422.442	1.399	0.0113	1.397	0.0112	1.403	0.0114	1.399	0.0121
426.300	1.402	0.0110	1.401	0.0108	1.406	0.0111	1.403	0.0118
430.158	1.405	0.0108	1.404	0.0105	1.409	0.0108	1.406	0.0116
434.017	1.408	0.0104	1.407	0.0102	1.412	0.0105	1.409	0.0116
437.875	1.411	0.0101	1.410	0.0100	1.416	0.0104	1.412	0.0114
441.733	1.415	0.00989	1.414	0.00978	1.419	0.0103	1.415	0.0114
445.591	1.418	0.00962	1.417	0.00966	1.422	0.0103	1.418	0.0114
449.449	1.421	0.00961	1.420	0.00959	1.425	0.0101	1.421	0.0114
453.307	1.424	0.00952	1.423	0.00963	1.428	0.0101	1.424	0.0114
457.165	1.427	0.00952	1.426	0.00959	1.430	0.0101	1.427	0.0115
461.023	1.430	0.00957	1.429	0.00974	1.433	0.0101	1.430	0.0114
464.881	1.432	0.00965	1.432	0.00976	1.436	0.0101	1.433	0.0115
468.739	1.435	0.00943	1.434	0.00985	1.439	0.0102	1.435	0.0115
472.597	1.438	0.00932	1.437	0.00991	1.442	0.0101	1.438	0.0116
476.455	1.441	0.00914	1.440	0.00994	1.445	0.0101	1.441	0.0116
480.313	1.444	0.00922	1.443	0.0101	1.448	0.0105	1.444	0.0118
484.171	1.447	0.00943	1.445	0.0101	1.450	0.0107	1.447	0.0120
488.029	1.450	0.00975	1.448	0.0103	1.453	0.0110	1.450	0.0123
491.887	1.453	0.0101	1.451	0.0104	1.456	0.0110	1.453	0.0127
495.745	1.456	0.0105	1.454	0.0105	1.459	0.0113	1.455	0.0128
499.603	1.458	0.0107	1.457	0.0106	1.462	0.0114	1.458	0.0130
503.462	1.461	0.0110	1.460	0.0107	1.465	0.0114	1.461	0.0133

Table 5. Continued

Frequency (cm^{-1})	146 K		156 K		166 K		176 K	
	n	k	n	k	n	k	n	k
507.320	1.464	0.0111	1.463	0.0108	1.468	0.0116	1.464	0.0133
511.178	1.467	0.0110	1.466	0.0110	1.471	0.0117	1.468	0.0134
515.036	1.470	0.0109	1.469	0.0111	1.475	0.0118	1.472	0.0137
518.894	1.474	0.0110	1.473	0.0112	1.478	0.0121	1.476	0.0141
522.752	1.478	0.0111	1.477	0.0115	1.483	0.0124	1.480	0.0148
526.610	1.482	0.0115	1.481	0.0119	1.488	0.0133	1.486	0.0167
530.468	1.487	0.0125	1.487	0.0134	1.493	0.0158	1.490	0.0205
534.326	1.492	0.0155	1.491	0.0171	1.497	0.0200	1.493	0.0248
538.184	1.496	0.0199	1.494	0.0211	1.499	0.0234	1.495	0.0283
542.042	1.498	0.0234	1.497	0.0240	1.502	0.0264	1.497	0.0309
545.900	1.501	0.0258	1.500	0.0258	1.505	0.0283	1.500	0.0336
549.758	1.502	0.0320	1.501	0.0334	1.507	0.0366	1.501	0.0405
553.616	1.502	0.0337	1.500	0.0349	1.506	0.0375	1.500	0.0428
557.474	1.502	0.0347	1.501	0.0357	1.506	0.0393	1.500	0.0438
561.332	1.503	0.0355	1.502	0.0365	1.507	0.0403	1.501	0.0450
565.190	1.504	0.0361	1.503	0.0376	1.509	0.0416	1.502	0.0459
569.048	1.506	0.0373	1.505	0.0385	1.509	0.0440	1.503	0.0476
572.906	1.508	0.0376	1.506	0.0392	1.510	0.0436	1.504	0.0475
576.765	1.510	0.0386	1.508	0.0399	1.512	0.0444	1.505	0.0484
580.623	1.512	0.0395	1.510	0.0408	1.514	0.0455	1.507	0.0495
584.481	1.514	0.0403	1.512	0.0419	1.516	0.0466	1.509	0.0502
588.339	1.517	0.0410	1.515	0.0427	1.518	0.0478	1.511	0.0513
592.197	1.519	0.0425	1.517	0.0440	1.521	0.0488	1.514	0.0528
596.055	1.522	0.0437	1.520	0.0451	1.523	0.0504	1.516	0.0538
599.913	1.524	0.0449	1.523	0.0466	1.525	0.0522	1.519	0.0558
603.771	1.527	0.0461	1.525	0.0485	1.528	0.0531	1.521	0.0580
607.629	1.530	0.0470	1.528	0.0503	1.530	0.0560	1.523	0.0592
611.487	1.533	0.0495	1.530	0.0517	1.532	0.0562	1.525	0.0606
615.345	1.535	0.0504	1.533	0.0527	1.536	0.0567	1.528	0.0635
619.203	1.538	0.0522	1.536	0.0549	1.539	0.0618	1.530	0.0658
623.061	1.542	0.0534	1.539	0.0572	1.540	0.0652	1.532	0.0682
626.919	1.545	0.0554	1.542	0.0578	1.542	0.0643	1.534	0.0710
630.777	1.548	0.0571	1.545	0.0603	1.546	0.0670	1.536	0.0717
634.635	1.552	0.0592	1.548	0.0621	1.548	0.0698	1.539	0.0755
638.493	1.556	0.0607	1.552	0.0640	1.551	0.0707	1.541	0.0770
642.351	1.561	0.0633	1.556	0.0661	1.555	0.0744	1.543	0.0806
646.209	1.566	0.0667	1.561	0.0690	1.557	0.0779	1.545	0.0826
650.067	1.573	0.0682	1.566	0.0727	1.559	0.0802	1.544	0.0879

at 150 K in Figs. 10 and 11. The real indices of refraction are compared in Figs. 10(a) and 10(b). The difference in n between our results and those of Trotta[23] varies between −5 and +27%, while we remain within ~10% of Johnson and Atreya[4] for the frequency range 500–100 cm^{-1}.

The imaginary indices of refraction are compared in Figs. 11(a)–11(c). The comparison in Fig. 11(b) is limited to the 300–150 cm^{-1} spectral region because the film thicknesses used by the Johnson and Atreya[4] and Trotta[23] studies are not adequate to obtain good data outside this region. The percent difference in k between our results and those of Trotta over a larger frequency range of 650–100 cm^{-1} [Fig. 11(c)] seems to vary relatively smoothly across the spectrum, gradually increasing in magnitude as the region of the 225 cm^{-1} band maximum is reached. The apparently large discrepancy at the band maximum of ~90% is consistent with the fact that our samples were formed by direct deposition whereas those of Trotta were prepared by warming a film initially deposited at a lower temperature.[17] In particular, the crystalline phase directly deposited spectra of Trotta (series II) differ from the warmed spectra (series I) in that the band strength of the 225 cm^{-1} band is almost twice that in the directly deposited case, whereas the 160 cm^{-1} band strength remains roughly the same, leading to a greater ratio of the 225–160 cm^{-1} band strengths for the directly deposited case. Furthermore, these bands are narrower in series II than in series I. As to whether the actual magnitude of the discrepancy can be fully attributed to these differences between the directly deposited and the warmed spectra is hard to assess since these effects have not been studied quantitatively.

Table 6. Peak Frequencies and Measured Absorbances of the 225 and 160 cm^{-1} Bands as a Function of Temperature[a]

Temperature (K)	225 cm^{-1} Band Peak Frequency (cm^{-1})	225 cm^{-1} Band Measured Absorbance	160 cm^{-1} Band Peak Frequency 160 cm^{-1}	160 cm^{-1} Band Measured Absorbance	Ratio of Absorbances 225 cm^{-1}/160 cm^{-1}
106	218	0.58	N/A[b]	N/A	N/A
116	218	0.59	N/A	N/A	N/A
126	218	0.66	N/A	N/A	N/A
136	218	1.27	160	0.28	4.53
146	218	1.34	160	0.29	4.62
156	218	1.40	160	0.29	4.83
166	218	1.35	160	0.27	5.00
176	218	1.20	158	0.27	4.44

[a]Also shown is the ratio of the peak absorbances of the 225–160 cm^{-1} bands. Films roughly 5.3 μm thick were chosen at the various temperatures for this table.
[b]N/A, not applicable.

8. Conclusions

Optical constants of water ice films formed by direct deposition at temperatures between 106 and 176 K have been determined in the 50–650 cm^{-1} spectral region (λ = 15–200 λm). Water ice films up to ~140 μm thick (total film thickness of a double-sided film) were used to extract optical constants. Film thicknesses were determined by a combination of monitoring the thickness-dependent interference fringes in a He–Ne beam reflecting off the ice film surface at 45° and by following the thickness-

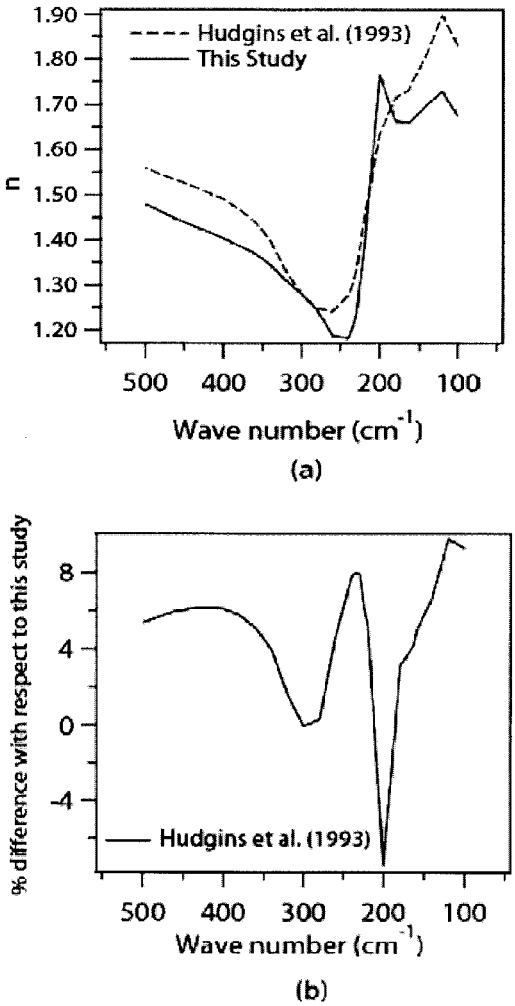

Fig. 8. (a) Comparison of our real indices of refraction at 106 K with those of Hudgins *et al.* (1993)[21] at 100 K. (b) Percentage differences of Hudgins *et al.* (1993)[21] relative to this study.

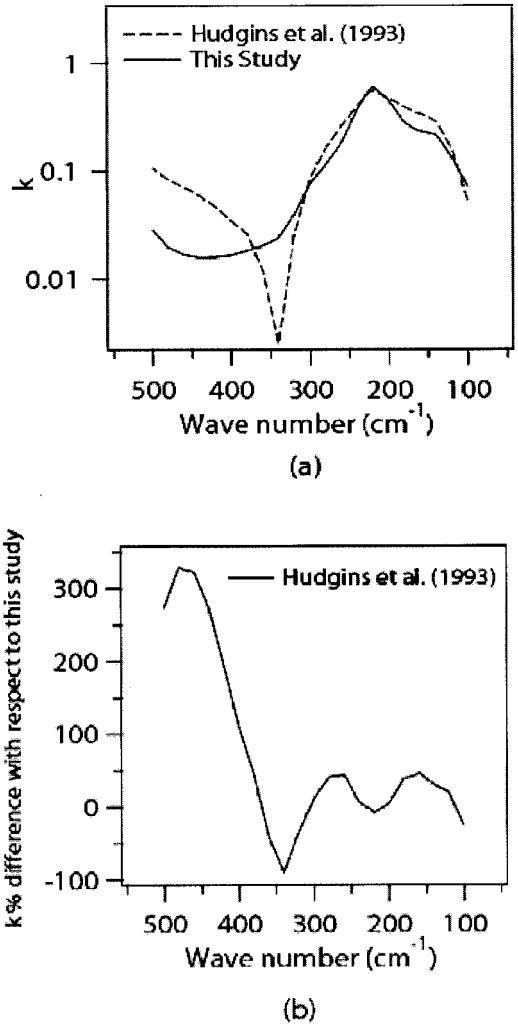

Fig. 9. (a) Comparison of our imaginary indices of refraction at 106 K with those of Hudgins *et al.* (1993)[21] at 100 K. (b) Percentage differences of Hudgins *et al.* (1993)[21] relative to this study.

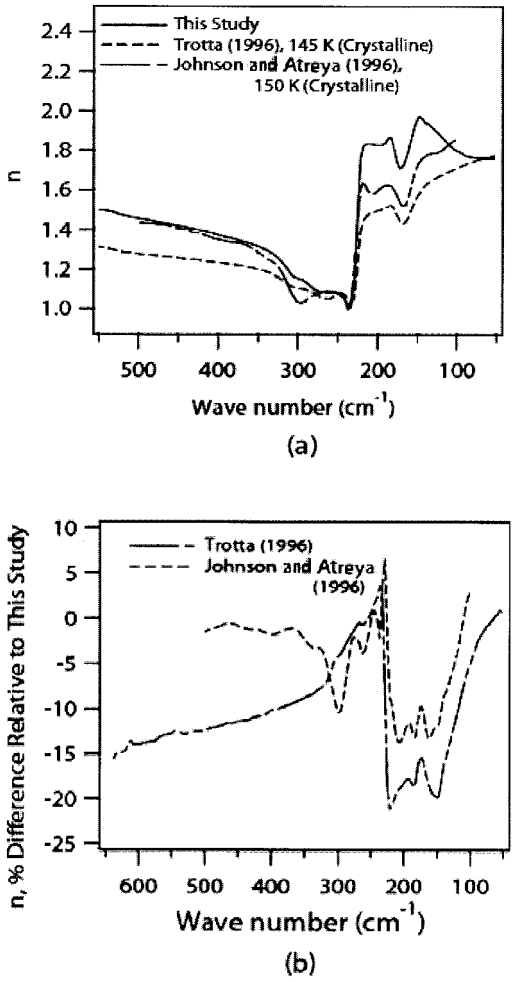

Fig. 10. (a) Comparison of our real indices of refraction at 146 K with those of Johnson and Atreya (1996)[4] (150 K) and those of Trotta (1996)[23] (145 K). (b) The percentage differences of Johnson and Atreya (1996)[4] and Trotta (1996)[23] relative to this study.

dependent oscillations in the measured absorbance at 500 cm^{-1} as a function of film growth. Our optical constants have been compared with other measurements available at comparable temperatures. In the frequency regions of high absorbance, k was too large in some previous data sets to have been accurately measured. Conversely, in the frequency regions of low absorbance, k was too low to have been measured accurately. In some cases the observed discrepancies between this study and previous measurements could be explained qualitatively in terms of the different thermal histories of the samples used in the various studies. However, the actual magnitude of the discrepancies across this spectral range can be discussed only when the effect of thermal history and experimental conditions on the far-IR spectrum of water ice has been studied quantitatively. For example, the substrate affects the transition point between amorphous and crystalline ice, and annealing a film of amorphous ice may result in a film that does not completely convert to crystalline ice over relatively short time scales. Since our films were deposited at

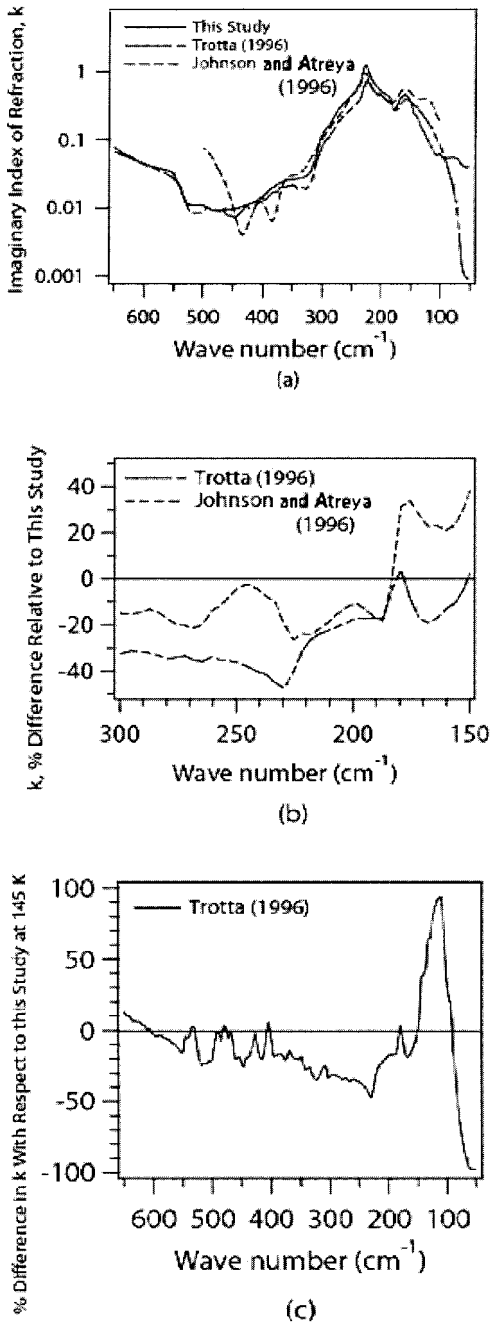

Fig. 11. (a) Comparison of our imaginary indices of refraction at 146 K with those of Johnson and Atreya (1996)[4] (150 K) and those of Trotta (1996)[23] (145 K). (b) Percentage differences of Johnson and Atreya (1996)[4] and Trotta (1996)[23] in the 150–300 cm^{-1} region relative to our study. (c) Percentage differences of Trotta (1996)[23] relative to the imaginary indices of this study in the 100–650 cm^{-1} region.

the temperature of the measurements, they should be relevant for geophysical and astronomical studies.

References

1. K. N. Liou, "Influence of cirrus clouds on weather and climate processes: a global perspective," Mon. Weather Rev. **114,** 1167–1199 (1986).
2. G. L. Stephens, S. C. Tsay, P. W. Stackhouse, and P. J. Flatau,

"The relevance of the microphysical and radiative properties of cirrus clouds to climate and climatic feedback," J. Atmos. Sci. **47,** 1742–1753 (1990).
3. S. G. Warren, "Optical constants of ice from the ultraviolet to the microwave," Appl. Opt. **23,** 1206–1225 (1984).
4. B. R. Johnson and S. K. Atreya, "Feasibility of determining the composition of planetary ices by far infrared observations: application to Martian cloud and surface ices," Icarus **119,** 405–426 (1996).
5. B. Schmitt, E. Quirico, F. Trotta, and W. M. Grundy, "Optical properties of ices from UV to infrared," in *Solar System Ices*, B. Schmitt, C. de Bergh, and M. Festov, eds. (Kluwer Academic, 1998), pp. 199–250.
6. A. A. Simon-Miller, B. Conrath, P. J. Gierasch, and R. F. Beebe, "A detection of water ice on Jupiter with Voyager IRIS," Icarus **145,** 454–461 (2000).
7. E. Dartois, P. Cox, P. R. Roelfsema, A. P. Jones, A. Tielens, L. d'Hendecourt, M. J. de Muizon, B. Schmitt, T. Lim, B. Swinyard, and A. M. Heras, "Detection of the 44 μm band of water ice in absorption in combined ISO SWS-LWS spectra," Astron. Astrophys. **338,** L21–L24 (1998).
8. J. C. Augereau, A. M. Lagrange, D. Mouillet, J. C. B. Papaloizou, and P. A. Grorod, "On the HR 4796 A circumstellar disk," Astron. Astrophys. **348,** 557–569 (1999).
9. S. Molinari, C. Ceccarelli, G. J. White, P. Saraceno, B. Nisini, T. Giannini, and E. Caux, "Detection of the 62 micron crystalline H_2O ice feature in emission toward HH 7 with the Infrared Space Observatory long-wavelength spectrometer," Astrophys. J. **521,** L71–L74 (1999).
10. K. Malfait, C. Waelkens, J. Bouwman, A. De Koter, and L. Waters, "The ISO spectrum of the young star HD 142527," Astron. Astrophys. **345,** 181–186 (1999).
11. F. J. Molster, L. Waters, N. R. Trams, H. van Winckel, L. Decin, J. T. van Loon, C. Jager, T. Henning, H. U. Kaufl, A. De Koter, and J. Bouwman, "The composition and nature of the dust shell surrounding the binary AFGL 4106," Astron. Astrophys. **350,** 163–180 (1999).
12. A. Coustenis, B. Schmitt, R. K. Khanna, and F. Trotta, "Plausible condensates in Titan's stratosphere from Voyager infrared spectra," Planet. Space Sci. **47,** 1305–1329 (1999).
13. More information about the ISO mission can be obtained at isowww.estec.esa.nl/.
14. More information about the SIRTF mission can be obtained at sirtf.caltech.edu.
15. More information about the SOFIA mission can be obtained at sofia.arc.nasa.gov/.
16. J. Bertie, H. Labbe, and E. Whalley, "Absorptivity of ice I in the range 4000–30 cm^{-1}," J. Chem. Phys. **50,** 4501–4520 (1969).
17. R. G. Smith, G. Robinson, A. R. Hyland, and G. L. Carpenter, "Molecular ices as temperature indicators for interstellar dust—the 44 μm4 and 62 μm lattice features of H_2O ice," Mon. Not. R. Astron. Soc. **271,** 481–489 (1994).
18. M. M. Maldoni, G. Robinson, R. G. Smith, W. W. Duley, and A. Scott, "Measurements of the 44 μm band of H_2O ice deposited on amorphous carbon and amorphous silicate substrates," Mon. Not. R. Astron. Soc. **309,** 325–331 (1999).
19. M. H. Moore and R. L. Hudson, "Far-infrared spectral studies of phase-changes in water ice induced by proton irradiation," Astrophys. J. **401,** 353–360 (1992).
20. M. H. Moore, R. L. Hudson, and P. A. Gerakines, "Mid- and far-infrared spectroscopic studies of the influence of temperature, ultraviolet photolysis and ion irradiation on cosmic-type ices," Spectrochim. Acta Part A **57,** 843–858 (2001).
21. D. Hudgins, S. Sandford, L. Allamandola, and G. Tielens, "Mid- and far-infrared spectroscopy of ices: optical constants and integrated absorbances," Astrophys. J. Suppl. Ser. **86,** 713–770 (1993).
22. J. E. Bertie and S. M. Jacobs, "Far-infrared adsorption by ices Ih and Ic at 4.3 K and the powder diffraction pattern of ice Ic," J. Chem. Phys. **67,** 2445–2448 (1977).
23. F. Trotta, "Determination des constantes optiques de glaces dans l'infrarouge moyen et lontain. Application aux grains du milieu interstellaire et des enveloppes curcumstellaires," Ph.D. dissertation (Universite Joseph Fourier, Grenoble, France, 1996).
24. O. B. Toon, M. A. Tolbert, B. G. Koehler, A. M. Middlebrook, and J. Jordan, "Infrared optical-constants of H_2O ice, amorphous nitric-acid solutions, and nitric-acid hydrates," J. Geophys. Res. **99D,** 25631–25654 (1994).
25. M. M. Maldoni, R. G. Smith, G. Robinson, and V. L. Rookyard, "A study of the 2.5–25 μm spectrum of H_2O ice," Mon. Not. R. Astron. Soc. **298,** 251–258 (1998).
26. B. Rajaram, D. L. Glandorf, D. B. Curtis, M. A. Tolbert, O. B. Toon, and N. Ockman, "Temperature-dependent optical constants of water ice in the near infrared: new results and critical review of the available measurements," Appl. Opt. **40,** 4449–4462 (2001).
27. M. L. Clapp, R. E. Miller, and D. R. Worsnop, "Frequency-dependent optical-constants of water ice obtained directly from aerosol extinction spectra," J. Phys. Chem. **99,** 6317–6326 (1995).
28. R. T. Tisdale, D. L. Glandorf, M. A. Tolbert, and O. B. Toon, "Infrared optical constants of low-temperature H_2SO_4 solutions representative of stratospheric sulfate aerosols," J. Geophys. Res. **103D,** 25353–25370 (1998).
29. J. Marti and K. Mauersberger, "A survey and new measurements of ice vapor-pressure at temperatures between 170 and 250 K," Geophys. Res. Lett. **20,** 363–366 (1993).
30. G. P. Johari, "The spectrum of ice," Contemp. Phys. **22,** 613–642 (1981).
31. O. Mishima, D. D. Klug, and E. Whalley, "The far-infrared spectrum of ice Ih in the range 8–cm^{-1}: sound-waves and difference bands, with application to Saturns rings," J. Chem. Phys. **78,** 6399–6404 (1983).
32. M. A. Zondlo, T. B. Onasch, M. S. Warshawsky, M. A. Tolbert, G. Mallick, P. Arentz, and M. S. Robinson, "Experimental studies of vapor-deposited water-ice firms using grazing-angle FTIR-reflection absorption spectroscopy," J. Phys. Chem. B **101,** 10887–10895 (1997).
33. D. F. Edwards, "Silicon (Si)," in *Handbook of Optical Constants of Solids*, E. D. Palik, ed. (Academic, 1985), p. 547.
34. B. S. Berland, D. E. Brown, M. A. Tolbert, and S. M. George, "Refractive index and density of vapor-deposited ice," Geophys. Res. Lett. **22,** 3493–3496 (1995).